# Tunable positive and negative refraction of infrared radiation in graphene-dielectric multilayers

R. Z. Zhang, and Z. M. Zhang

Citation: Appl. Phys. Lett. **107**, 191112 (2015); doi: 10.1063/1.4935797
View online: http://dx.doi.org/10.1063/1.4935797
View Table of Contents: http://aip.scitation.org/toc/apl/107/19
Published by the American Institute of Physics

# Tunable positive and negative refraction of infrared radiation in graphene-dielectric multilayers

R. Z. Zhang and Z. M. Zhang[a)]
*G.W. Woodruff School of Mechanical Engineering, Georgia Institute of Technology, Atlanta, Georgia 30332, USA*

(Received 6 August 2015; accepted 3 November 2015; published online 13 November 2015)

Graphene-dielectric multilayers consisting of alternating layers of atom-thick graphene and nanometer-scale dielectric films exhibit characteristics of hyperbolic metamaterials, in which one positive and one negative permittivity are defined for orthogonal directions. Negative permittivity for electric field polarized in the direction parallel to the conductive graphene sheets gives rise to a negative angle of refraction and low-loss transmission for the side-incidence perspective proposed in this work. The Poynting vector tracing demonstrates the switching between positive and negative refraction in the mid-infrared region by tuning the chemical potential of graphene. This adjustable dual-mode metamaterial holds promise for infrared imaging applications. © *2015 AIP Publishing LLC*. [http://dx.doi.org/10.1063/1.4935797]

Where the development of ultra-compact imaging and sensing devices in modern electronics is needed, nano- or micro-scale structured materials and surfaces can provide unique optical properties.[1,2] These engineered hyperbolic metamaterials can be tuned to control the transmission or absorption of electromagnetic waves. The subwavelength-regime components in metamaterials allow atypical guiding or directional control of light, designated as a negative angle of refraction.[3] The characteristic property of these materials is their uniaxial anisotropy and negative permittivity of one axial component, achieved by either patterning or depositing plasmonic materials.[4] Sub-micron thick dielectric and metal periodic layers or multilayers enable this hyperbolic dispersion.[1]

Metal-dielectric multilayers traditionally have many atoms-thick metal layers that could result in poor transmission of radiation. Graphene, which behaves as a two-dimensional (2D) conducting sheet, can substitute for these lossy layers. The charge carrier concentration or chemical potential of graphene can be tuned via voltage biasing or chemical doping.[5,6] The variance between electron states in graphene could imply selective or switchable transmission or absorption of radiation for infrared applications.[7] Several studies have shown unique radiative properties in similar graphene-dielectric multilayers, including cavity emission,[8] light absorption and modulation,[9–11] negative group velocity,[12,13] and nonlocal wave diffraction.[14] Here, we present an alternative perspective of the graphene-dielectric multilayers to better accomplish the sought-after optical properties of hyperbolic metamaterials. By introducing the side-incidence perspective, positive and negative refraction can be actively controlled.

The traditional perspective of the graphene-dielectric multilayers (top-incidence) is illustrated by the conical beam, and the proposed alternative perspective (side-incidence) is shown by the rhombic beam in Fig. 1(a). The unique advantage of the side-incidence perspective is the tunability between positive and negative refraction, enabled by graphene. Since all structures have characteristic dimensions that are magnitudes smaller than the wavelengths of interest, the stratified medium may appear homogeneous but anisotropic. Exact multilayer electromagnetic wave theory is used to validate the effective medium assumption for the

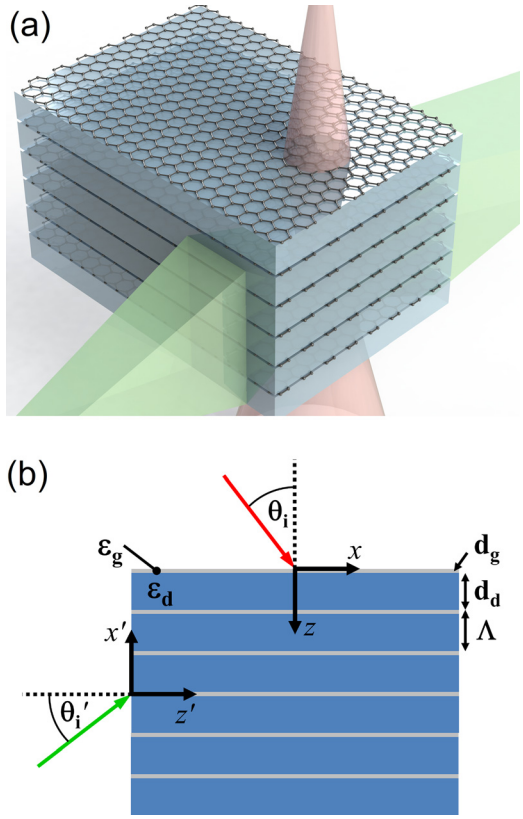


FIG. 1. Illustration of graphene-dielectric multilayers showing (a) the interactions with light beams in perpendicular directions (top-incidence versus side-incidence perspectives), and (b) the nomenclature of associated dimensions and permittivities of the graphene sheets and dielectric spacers. Coordinates and nomenclature corresponding to side-incidence are denoted by the prime.

[a)]Author to whom correspondence should be addressed. Electronic mail: zhuomin.zhang@me.gatech.edu. Tel.: 404-385-4225.

 

top-incidence case only. The associated nomenclatures of both orientations are denoted in Fig. 1(b).

The sheet conductivity ($\sigma$) of an ideal and flawless single-layer graphene sheet depends on the frequency ($\omega$), chemical potential ($\mu$), relaxation time ($\tau$), and temperature ($T$). In the frequency range corresponding to mid-infrared wavelengths, the intraband conductivity dominates, and behaves similar to the Drude model for electrons.[15,16] The effect from the inter-band conductivity term for direct electron transitions is nearly negligible given sufficiently high chemical potential (i.e., $\mu > 0.1$) and near room temperature ($T = 300\,\mathrm{K}$) for mid- to far-infrared considerations. The relaxation time is between $10^{-12}$ s and $10^{-13}$ s.[15,17] The expression for the dielectric permittivity of graphene is given by

$$\varepsilon_g = \varepsilon_d + \frac{i\sigma(\omega,\mu)}{\omega\varepsilon_0 d_g}, \tag{1}$$

where $d_g = 0.335\,\mathrm{nm}$ is the interlayer distance resolved from graphite.[18,19] The static and lossless permittivity for the dielectric spacer is $\varepsilon_d = 6.0$. These dielectric permittivities and their respective dimensions are indicated in Fig. 1(b). In this study, the dielectric spacer thickness is set between $d_d = 10\,\mathrm{nm}$ and $50\,\mathrm{nm}$. The surrounding media are semi-infinite vacuum ($\varepsilon = 1$).

The electromagnetic fields in every layer can be determined by the transfer matrix method (TMM) for isotropic homogeneous planar multilayers.[20,21] An algorithm has been formulated considering uniaxial anisotropic media for a multilayer slab using the effective medium theory (EMT).[22] The EMT method is a simple weighting of the permittivity parallel to the graphene-dielectric interfaces (ordinary direction), and the inverse perpendicular to the interfaces (extraordinary direction).[23,24] The expressions of the ordinary and extraordinary dielectric functions are given by

$$\varepsilon_O = f\varepsilon_g + (1-f)\varepsilon_d, \tag{2a}$$

$$\varepsilon_E = \varepsilon_d, \tag{2b}$$

where the filling ratio is $f = d_g/\Lambda$, given the period is $\Lambda = d_g + d_d$. Since graphene is much thinner than the dielectric spacer and behaves as a 2D conducting sheet, it has no contribution in the direction perpendicular to the interfaces.[6,9,18]

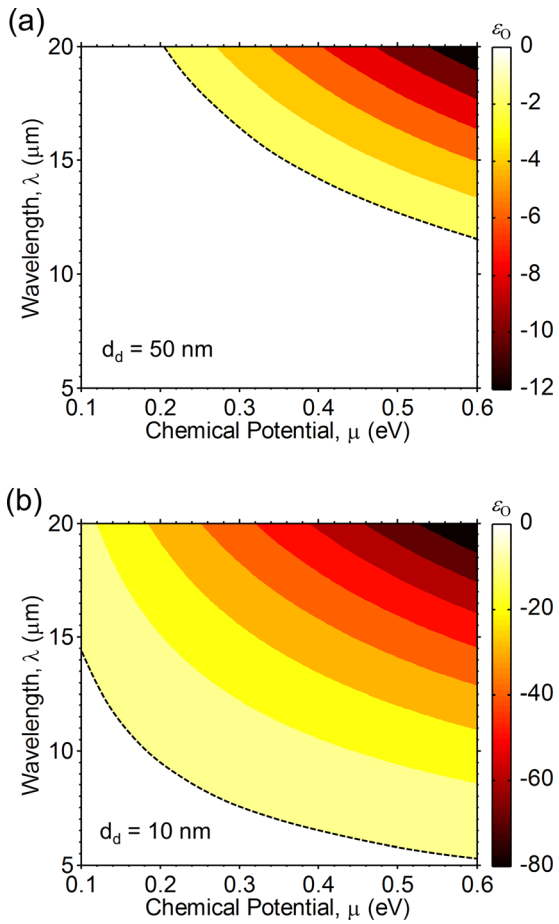


FIG. 2. Contour plots of the multilayer dielectric permittivity determined by effective medium theory (EMT). The dielectric spacer dimensions of (a) 50 nm and (b) 10 nm are shown. The dashed line marks where $\varepsilon_O = 0$. Positive $\varepsilon_O$ are not shaded in the lower-left region and rise monotonically toward $\varepsilon_d = 6.0$.

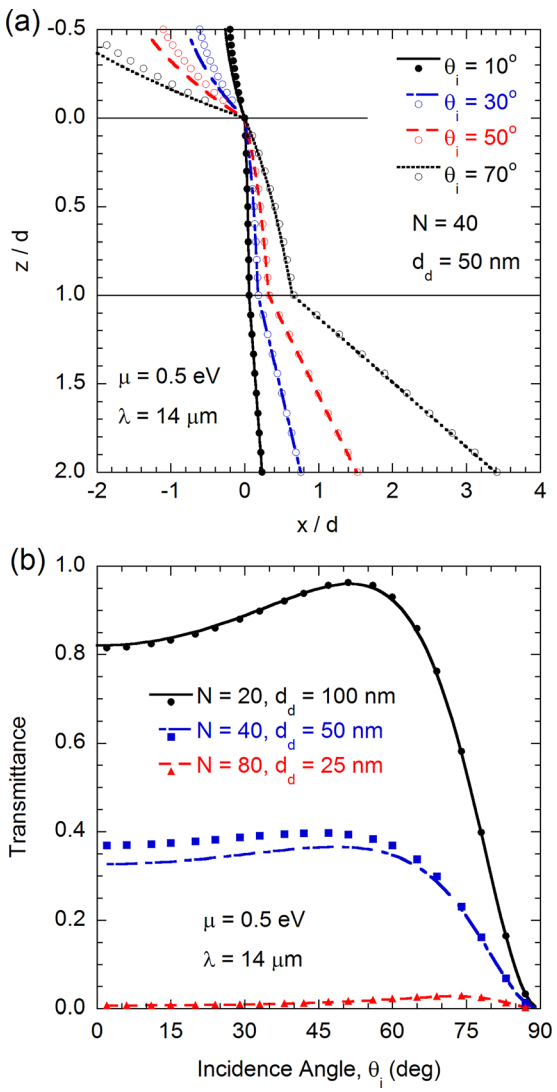


FIG. 3. The radiative properties determined by transfer matrix method (TMM, lines) versus EMT (points) of the top-incidence multilayers. (a) The energy streamlines in multilayer thin film with slab thickness of $d = 2.01\,\mu\mathrm{m}$. (b) Transmittance spectra of the multilayer thin film with different number of layer periods and dielectric spacer sizes.

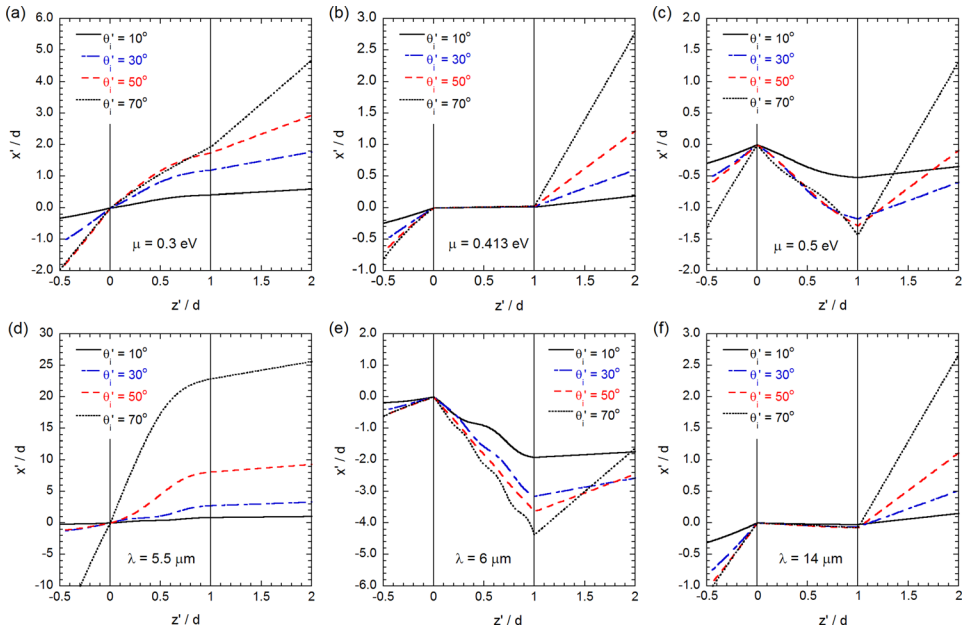


FIG. 4. Energy streamlines in graphene-dielectric multilayers from side-incidence perspective. Corresponding to $d_d = 50\,\text{nm}$ and $\lambda = 14\,\mu\text{m}$: (a), (b), and (c) exhibit positive index, epsilon-near-zero, and negative index dispersions, respectively, as the graphene chemical potential is increased. For $d_d = 10\,\text{nm}$ and $\mu = 0.5\,\text{eV}$: (d), (e), and (f) demonstrate large lateral shifts, negative index, and self-collimation, respectively, for increasing wavelength. The slab thickness ($d$) is set to $2.0\,\mu\text{m}$.

The ordinary direction permittivity ($\varepsilon_O$) of the graphene-dielectric multilayers calculated using EMT is shown in Fig. 2 for two different dielectric spacer thicknesses. The permittivity of the graphene sheet itself is always negative, and decreases monotonically by about an order magnitude from $\lambda = 5\,\mu\text{m}$ to $20\,\mu\text{m}$. Figure 2(a) shows, with 50 nm-thick dielectric spacers, $\varepsilon_O$ is negative when $\lambda > 11\mu\text{m}$. As the chemical potential of graphene decreases, the cutoff wavelength for negative $\varepsilon_O$ becomes higher, as indicated by the dashed line. This trend is shifted toward the lower-left when the dielectric spacer thickness is reduced to 10 nm, as seen in Fig. 2(b). Since the filling ratio is increased by five-fold, the effect from $\varepsilon_g$ becomes stronger, and negative $\varepsilon_O$ exists at wavelengths down to $\lambda = 5\,\mu\text{m}$. The magnitude of $\varepsilon_O$ is also increased approximately five-fold for the settings corresponding to the upper-right of the contoured plot. Any higher chemical potential in graphene may be limited by voltage biasing.[6,16,25]

To illustrate the possible negative index in the multilayers from the top-incidence perspective, the energy streamlines made by tracing the Poynting vectors are shown in Figure 3(a). Detailed discussions of the energy streamline method can be found in Refs. 21 and 22. The number of periods ($N$) is 40, and the dielectric spacer thickness is 50 nm, which gives the total slab thickness of $d = 2.01\mu\text{m}$. The streamlines determined by TMM (lines) and EMT (points) agree reasonably well under the prescribed parameters. For shorter wavelengths or thicker dielectric spacers, EMT breaks down, according to $|k_z d_d| \ll \pi$ or $2d_d \ll \lambda$.[18,23,24] Despite having negative $\varepsilon_O$ at the prescribed wavelength and chemical potential, no negative angle light bending is observed at any incidence angle ($\theta_i$). To better understand the wave interactions in transformational optics, two types of hyperbolic dispersion are characterized. The hyperbolic dispersion equation for transverse-magnetic (TM) waves in the top-incidence perspective can be written as

$$\frac{k_x^2}{\varepsilon_O} + \frac{k_z^2}{\varepsilon_E} = k_0^2, \tag{3}$$

where $k_x = k_0 \sin(\theta_i)$.[23,26] In the case previously presented, $\varepsilon_O < 0$ and $\varepsilon_E > 1$ mean a large imaginary-termed $k_z$ for all propagating incident waves ($k_x < k_0$). Since $\varepsilon_O$ contains a small and positive imaginary term ($\varepsilon_O''$), the real component of the wavevector can be approximated as $k_z'^2 \approx k_0^2\varepsilon_O'' - k_x^2\varepsilon_O''/\varepsilon_E$. This dispersion relation follows the type II hyperbolic dispersion, which does not demonstrate negative angle refraction.[27,28] Fig. 3(b) demonstrates how shrinking the period size and adding the number of layers increases the influence of the negative-permittivity graphene and results in the loss of transmission through the multilayers containing many graphene sheets.

The side-incidence perspective in effect switches $k_z$ for $k_{x'}$, and $k_x$ for $k_{z'}$ in Eq. (3). This change in the dispersion relation supports negative angle refraction, while the metamaterial is still defined as type II hyperbolic. Under this circumstance, all incident waves on the multilayers result in Poynting vectors directed in the negative $x'$ direction.[23,26] The energy streamlines of the side-incidence multilayers are illustrated in Fig. 4 for various cases. The slab thickness $d$ in the direction of $z'$ is set to exactly $2.0\,\mu\text{m}$, and $N$ is sufficiently large to accommodate millimeters-wide beam sizes in the $x'$ direction. In this framework, the EMT formulation of a uniaxial slab is suitable since the wavelength versus period sizing inequality is satisfied. The interaction with TM waves in the $y'$-$z'$ plane of incidence (magnetic field is in the $x'$ direction) is isotropic and high loss, according to $k_{x'}^2 + k_{z'}^2 = \varepsilon_O k_0^2$, and therefore not considered in this study.

Figures 4(a), 4(b), and 4(c) show the shift in dispersion type as the chemical potential is increased from $\mu = 0.3\,\text{eV}$, $0.413\,\text{eV}$, to $0.5\,\text{eV}$, respectively. In these cases, the dielectric spacer thickness ($d_d = 50\,\text{nm}$) and wavelength ($\lambda = 14\,\mu\text{m}$) are held constant. For $\mu = 0.3\,\text{eV}$ corresponding to positive $\varepsilon_O$, ordinary positive refraction is seen. At the dashed line indicated in Fig. 2(a), where the real part of $\varepsilon_O$ is zero ($\varepsilon_O'' = 0$), setting $\mu = 0.413\,\text{eV}$ makes the multilayers behave as a self-collimator. While this mode may promise fiber optic-like properties, it is extremely narrowband and suffers from high loss, which will be elaborated later. At

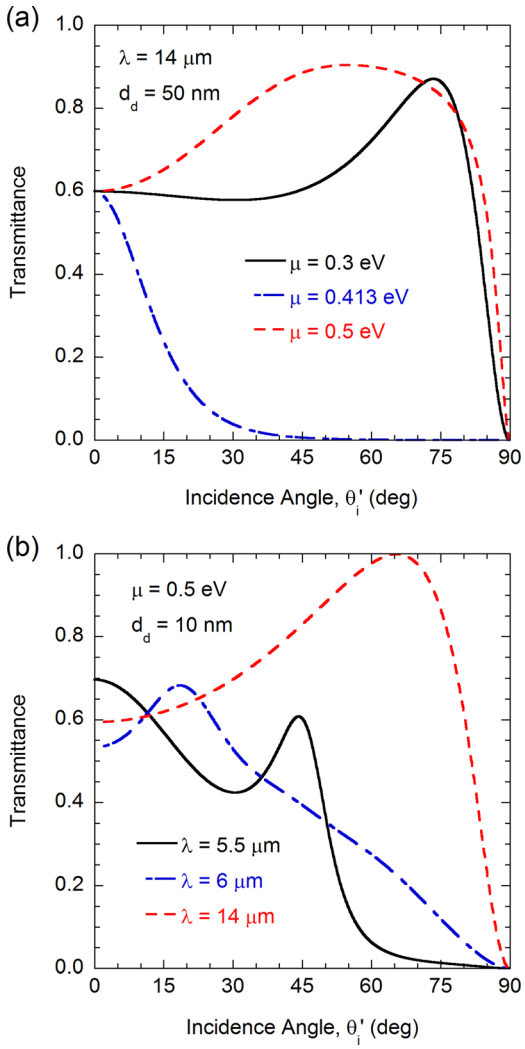


FIG. 5. Transmittance spectra of 2.0 $\mu$m-thick side-incidence graphene multilayer thin films corresponding to changing (a) graphene chemical potential and (b) wavelength.

$\mu = 0.5$ eV, where $\varepsilon_O = -1.28 + 0.13i$, the energy streamlines begin to divert in the negative $x'$ direction inside the medium. Some interference effects or undulations in the streamlines are observed, which may present some difficulty for applications in focusing and imaging.

The dielectric spacer size of $d_d = 10$ nm is used to illustrate the effect of largely negative $\varepsilon_O$ as the wavelength is increased. Figures 4(d), 4(e), and 4(f) show streamlines at $\lambda = 5.5$ $\mu$m, 6 $\mu$m, and 14 $\mu$m, respectively, while holding $\mu$ at 0.5 eV. At $\lambda = 5.5$ $\mu$m, the positive refraction is similar to that shown in Fig. 4(a), but with greater lateral shift. This is due to the small and positive real component in $\varepsilon_O$, thus amplifying the changes in the $z'$-component on the $x'$-component. In the case when $\lambda = 6$ $\mu$m, the streamlines present themselves similarly to those in Fig. 4(c) since $\varepsilon_O$ is also negative. When taking the wavelength to $\lambda = 14$ $\mu$m, where $\varepsilon_O = -29.3 + 0.65i$, the large magnitude in $\varepsilon_O$ makes $k_{x'}$ nearly insensitive to $k_{z'}$. This results in a self-collimation effect in the multilayer medium that is also broadband in longer mid-infrared wavelengths.[29] Unlike the collimation seen in Fig. 4(b), radiative transmission is sustained, as will be elaborated next.

The transmittance profiles with incidence angle for each case examined in Fig. 4 are shown in Fig. 5. The thin film is highly transmitting in both positive and negative refraction modes, as seen in Fig. 5(a). However, transmittance is almost totally lost at oblique angles when $\mu = 0.413$ eV. This epsilon-near-zero (ENZ) mode suffers from short penetration depths, approximated to be $\delta \approx \sqrt{\varepsilon_O''}/(2k_{x'}\sqrt{\varepsilon_E})$. Contrary to intuition, the penetration depth could be larger at ENZ by using a lossy dielectric that increases $\varepsilon_O''$.[29] In Fig. 5(b), the loss in transmittance accompanied by large lateral shift for incidence angles greater than approximately 60° is due to the near-ENZ mode when $\lambda = 5.5$ $\mu$m. Here, the anisotropic medium critical angle is defined by $\theta_c' = \sin^{-1}(\sqrt{\varepsilon_O})$, which gives $\theta_c' = 60.3°$.[20,29] The other two wavelengths far from ENZ demonstrate relatively good transmittance at oblique angles, with some interference patterns due to internal film reflections. Having a dielectric spacer defined by a real material dielectric function could allow highly penetrating radiation even toward the far-infrared wavelength regime.

A possible material for use as the dielectric layer is hexagonal boron nitride (hBN), which shares similar crystallographic hexagonal lattices with graphene and can be deposited in thin layers of a few nanometers to encapsulate transferred graphene sheets.[19,30–33] Outside the two narrow lattice vibration bands, the anisotropy in hBN is small and the dielectric function is about 6, as used in the present study.[30] It should be noted that reducing the dielectric index to $n = 1.5$ $(\varepsilon = 2.2)$ allows for negative $\varepsilon_O$ in the near-infrared regimes. On the other hand, if the dielectric layer is optically dense (i.e., $\varepsilon = 12$), the positive-to-negative permittivity occurs in the far-infrared. In order to fabricate the graphene-dielectric multilayers used in the side-incidence manner, further development of growth techniques that ensures multiple uniform and large area interface contacts between the dielectric spacer and graphene is needed. Works on vertically standing graphene "nanopetals" are encouraging developments toward the assembly of the graphene-dielectric multilayers.[34]

In summary, the graphene-dielectric multilayers demonstrate negative angle of refraction not in the traditional top-incidence orientation. Depending on the chemical potential or voltage biasing of the parallel graphene sheets, the effective anisotropic permittivity of the medium may be positive or negative. Energy streamlines traced from side-incidence shows both positive and negative refraction in infrared wavelengths. Generally, the graphene-dielectric multilayers can become negative refraction with increased chemical potential and toward longer mid-infrared wavelengths. With improved technology for growing the graphene-dielectric multilayer films in the desired orientation, this work holds promise in transparent subwavelength infrared imaging and filtering devices.

The authors gracefully acknowledge support from the National Science Foundation (CBET-1235975).

[1]A. Poddubny, I. Iorsh, P. Belov, and Y. Kivshar, Nat. Photonics **7**, 948 (2013).
[2]J. Sun, N. M. Litchinitser, and J. Zhou, ACS Photonics **1**, 293 (2014).
[3]Z. M. Zhang and C. J. Fu, Appl. Phys. Lett. **80**, 1097 (2002).

[4]A. A. High, R. C. Devlin, A. Dibos, M. Polking, D. S. Wild, J. Perczel, N. P. de Leon, M. D. Lukin, and H. Park, Nature **522**, 192 (2015).
[5]F. Schedin, A. K. Geim, S. V. Morozov, E. W. Hill, P. Blake, M. I. Katsnelson, and K. S. Novoselov, Nat. Mater. **6**, 652 (2007).
[6]K. S. Novoselov, A. K. Geim, S. V. Morozov, D. Jiang, Y. Zhang, S. V. Dubonos, I. V. Grigorieva, and A. A. Firsov, Science **306**, 666 (2004).
[7]A. Vakil and N. Engheta, Science **332**, 1291 (2011).
[8]I. V. Iorsh, I. S. Mukhin, I. V. Shadrivov, P. A. Belov, and Y. S. Kivshar, Phys. Rev. B **87**, 075416 (2013).
[9]I. S. Nefedov, C. A. Valaginnopoulos, and L. A. Melnikov, J. Opt. **15**, 114003 (2013).
[10]B.-Z. Xu, C.-Q. Gu, Z. Li, and Z.-Y. Niu, Opt. Express **21**, 23803 (2013).
[11]I. Khromova, A. Andryieuski, and A. Lavrinenko, Laser Photonics Rev. **8**, 916 (2014).
[12]D. Smirnova, P. Buslaev, I. Iorsh, I. V. Shadrivov, P. A. Belov, and Y. S. Kivshar, Phys. Rev. B **89**, 245414 (2014).
[13]K. V. Sreekanth, A. De Luca, and G. Strangi, Appl. Phys. Lett. **103**, 023107 (2013).
[14]R.-L. Chern and D. Han, Opt. Express **22**, 4817 (2014).
[15]M. Jablan, H. Buljan, and M. Soljačić, Phys. Rev. B **80**, 245435 (2009).
[16]L. A. Falkovsky, J. Phys.: Conf. Ser. **129**, 012004 (2008).
[17]Y. W. Tan, Y. Zhang, K. Bolotin, Y. Zhao, S. Adam, E. H. Hwang, S. Das Sarma, H. L. Stormer, and P. Kim, Phys. Rev. Lett. **99**, 246803 (2007).
[18]M. A. K. Othman, C. Guclu, and F. Capolino, Opt. Express **21**, 7614 (2013).
[19]B. Sachs, T. O. Wehling, M. I. Katsnelson, and A. I. Lichtenstein, Phys. Rev. B **84**, 195414 (2011).
[20]P. Yeh, *Optical Waves in Layered Media* (Wiley, New York, 2005).
[21]Z. M. Zhang, *Nano/Microscale Heat Transfer* (McGraw-Hill, New York, 2007).
[22]R. Z. Zhang and Z. M. Zhang, J. Quant. Spectrosc. Radiat. Transfer **158**, 91 (2015).
[23]J. Schilling, Phys. Rev. E **74**, 046618 (2006).
[24]O. Kidwai, S. V. Zhukovsky, and J. E. Sipe, Phys. Rev. A **85**, 053842 (2012).
[25]Z. Q. Li, E. A. Henriksen, Z. Jiang, Z. Hao, M. C. Martin, P. Kim, H. L. Stormer, and D. N. Basov, Nat. Phys. **4**, 532 (2008).
[26]L. Sun, S. Feng, and X. Yang, Appl. Phys. Lett. **101**, 241101 (2012).
[27]C. L. Cortes, W. Newman, S. Molesky, and Z. Jacob, J. Opt. **14**, 063001 (2012).
[28]Y. Guo, C. L. Cortes, S. Molesky, and Z. Jacob, Appl. Phys. Lett. **101**, 131106 (2012).
[29]S. Feng, Phys. Rev. Lett. **108**, 193904 (2012).
[30]R. Geick, C. H. Perry, and G. Rupprecht, Phys. Rev. **146**, 543 (1966).
[31]C. R. Dean, A. F. Young, I. Meric, C. Lee, L. Wang, S. Sorgenfrei, K. Watanabe, T. Taniguchi, P. Kim, K. L. Shepard, and J. Hone, Nat. Nanotechnol. **5**, 722 (2010).
[32]A. Kumar, T. Low, K. H. Fung, P. Avouris, and N. X. Fang, Nano Lett. **15**, 3172 (2015).
[33]A. Woessner, M. B. Lundeberg, Y. Gao, A. Principi, P. Alonso-González, M. Carrega, K. Watanabe, T. Taniguchi, G. Vignale, M. Polini, J. Hone, R. Hillenbrand, and F. H. L. Koppens, Nat. Mater. **14**, 421 (2015).
[34]H. Bao, A. Kumar, Y. Cai, Y. Ji, T. S. Fisher, and X. Ruan, J. Quant. Spectrosc. Radiat. Transfer **158**, 84 (2015).